

Diaza-adamantane derivatives as corrosion inhibitor for copper in nitric acid medium

G. Karthik · M. Sundaravadivelu · P. Rajkumar · M. Manikandan

Received: 30 June 2014 / Accepted: 9 October 2014 / Published online: 19 October 2014
© Springer Science+Business Media Dordrecht 2014

Abstract The effect of newly synthesized 6-hydroxy-5,7-diphenyl-1,3-diazaadamantane (HDDA) and 5,7-diphenyl-1,3-diazaadamantan-6-one (DDA) against the corrosion of copper in 1 M HNO_3 solution was investigated using potentiodynamic polarization, electrochemical impedance spectroscopy (EIS) and weight loss measurements. These measurements show that the inhibition efficiency (IE %) obtained by these compounds increased by increasing their concentrations, and maximum IE % to 90.84 % for HDDA and 89.87 % for DDA were found at 300 ppm. Data obtained from EIS studies were analyzed by an equivalent circuit model. EIS plots indicated that the inhibitor performance depends on the adsorption of the molecules on the metal surface. Polarization measurements showed that both HDDA and DDA are mixed-type but predominantly cathodic in 1 M HNO_3 solution. The adsorption of inhibitors on the copper surface from the nitric acid follows the Langmuir adsorption isotherm with a negative value of free energy, and these values indicated that adsorption of both HDDA and DDA molecules adsorbs physically on the copper surface. The surface morphology was examined by scanning electron microscope and atomic force microscope. Further, theoretical calculations were carried out and relationships between computed parameters and experimental IE % were discussed. All the results confirmed that e HDDA showed better efficiency in 1 M HNO_3 compared to DDA.

Keywords Copper corrosion · 1 M HNO_3 media · Diaza-adamantane derivatives · Electrochemical studies · Theoretical studies · SEM and AFM

G. Karthik · M. Sundaravadivelu (✉) · P. Rajkumar · M. Manikandan
Department of Chemistry, The Gandhigram Rural Institute - Deemed University,
Gandhigram 624 302, Tamil Nadu, India
e-mail: msundargri@gmail.com; msundar_gri@yahoo.com

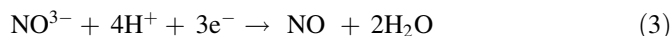
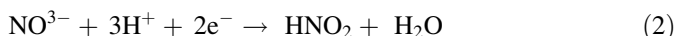
Introduction

Copper has many industrial applications because of its excellent corrosion resistance properties as well as its superior electrical and thermal performance. Thus, recent investigators have been attracted by the copper corrosion and its inhibition. Nitrogen-containing organic compounds such as amines and heterocyclic compounds are used as inhibitors for protecting the copper surface from corrosion in aggressive acid solutions. The inhibition efficiency depends on the chemical composition, structure and electronic parameters of the inhibitor, on the nature of the metal, and on the properties of the medium. Recently, organic inhibitors have been preferred to mineral ones because of their environmental safety and also for their excellent inhibitory properties. However, not just any chemical compound can be used as corrosion inhibitor. There are some requirements that the compound must fulfill in order to do so. An organic compound must have some features that give it the ability to act as a corrosion inhibitor, such as the number of adsorption sites and their charge density, molecular size, mode of interaction with the metal surface, and the formation of metallic complexes [1].

Copper is corroded in HNO_3 solutions and gives Cu^{2+} ions, which indicates that no oxide film is formed to protect the surface from the attack of the corrosive medium. Copper dissolution is thus expected to be the dominant reaction in the HNO_3 solution. The electrochemical reaction for copper in 1 M HNO_3 solution was also described by Joseph and Joseph as follows [2]: Anodic reaction:



Cathodic reactions:



Most of the N-heterocyclic compounds have shown mixed-type corrosion inhibition in acidic solutions for protection of metal surfaces [3, 4], while there are some studies indicating that cathodic inhibition is predominant [5]. It is generally assumed that the adsorption of an inhibitor at the metal/solution interface may take place via four types of mechanism during inhibition: (1) electrostatic attraction between charged molecules and the charged metal, (2) interaction of unshared electron pairs in the molecule with the metal, (3) interaction of π -electrons with the metal, and (4) a combination of the above [6, 7].

Many authors have shown interest in azole derivatives as inhibitors in the corrosion inhibition of copper metal in various acid solutions [8–11]. Niamien et al. studied the 2-mercaptobenzimidazole and 2-thiobenzylbenzimidazole in copper corrosion in a 1-M nitric acid solution with IE % to 90 and 87.7 % at 1.0 mM [12]. The inhibitory effects of thiamine hydrochloride on the corrosion of copper in a 2.5-M nitric acid solution was investigated by Abiola et al. [13] with 70 % efficiency at

1.0 mM. The effect of 2-hydroxyacetophenone-aroyl hydrazone derivatives on copper in a nitric acid solution were studied by Fouada et al. [14] with 94 % at 1.0 mM. Investigation of the corrosion of copper by quinoxaline derivatives in nitric acid solution by Zarrouk et al. [15] showed maximum IE % of 82.9 % at 1.0 mM. Zarrouk et al. [16] studied pyridazine derivatives on the corrosion of copper in nitric acid resulting in 82–96 % efficiency at 1.0 mM. Many authors have been investigating the various forms of monocyclic piperidine moiety in different acid environments [17–21], but no work has been reported for inhibiting action of the bicyclic bisbidine and tricyclic adamantane moiety. Use of diaza-adamantane derivatives as a new type of corrosion inhibitors for copper in nitric acid medium is reported here.

The intention of this work was to study the influence of two selected diazaadamantanes, namely 6-hydroxy-5,7-diphenyl-1,3-diazaadamantane (HDDA) and 5,7-diphenyl-1,3-diazaadamantan-6-one (DDA) on the inhibition of copper corrosion in 1 M HNO₃ solutions using electrochemical techniques, such as electrochemical impedance spectroscopy (EIS), Tafel polarization, weight loss, and quantum chemical calculation to explore the adsorption mechanism of diazaadamantane derivatives. Also, as the electronic structure of diazaadamantanes could be involved in determining interactions with the copper surface, the correlation between molecular calculations and inhibitor efficiencies was sought.

Materials and methods

Inhibitor synthesis and characterization

Synthesis of 5,7-diphenyl-1,3-diazaadamantan-6-one

A mixture of 1,3-diphenyl acetone (5.6 ml), para-formaldehyde (4.2 g), dry ammonium acetate (4 g), ammonium carbonate (2.7 g) and isopropanol was refluxed on a water bath with constant shaking for about 3–4 h. The flask was immediately cooled under tap water. Ether was added to the cooled reaction mixture and the precipitated 5,7-diphenyl 1,3-diazaadamantan-6-one was removed by filtration. It was recrystallized from chloroform. The yield was 1.9 gm, (55 %) with 264–266 °C mp.

Synthesis of 6-hydroxy-5,7-diphenyl-1,3-diazaadamantane

Sodium borohydride (2 g) was taken and dissolved in a minimum amount of water in a 100-ml round-bottom flask. To this, a solution of 5,7-diphenyl-1,3-diazaadamantanone (2 g) in isopropanol (100 ml) was added. This mixture was refluxed over a steam bath for 3 h. The reaction mixture was poured into a small amount of ice and the resulting solid was collected by filtration. Finally, 6-hydroxy-5,7-diphenyl-1,3-diazaadamantane was crystallized from chloroform. The yield was 1.76 gm, (88 %) with 254 °C mp. All the above inhibitors were prepared by the methods described in the literature [22].

Characterization

A NMR spectrum was recorded on a 300 MHz Bruker NMR spectrometer with TMS as the internal standard. Chemical shift values are presented in δ scale. IR spectra were recorded on a JASCO (FTIR 460 plus; Japan) spectrophotometer by using a KBr pellet.

The IR spectrum of the ketone (DDA) showed the strong absorption peak in 1,706.69 due to the carbonyl group. The hydroxyl group in the reduction product (HDDA) appeared at 3,511.74 and 3,475.1 cm^{-1} , while the carbonyl group at 1,706.69 cm^{-1} disappeared.

HDDA $^1\text{H-NMR}$: 7.249–7.386 (10H, phenyl protons, m), 3.792 (2H, s, $\text{C}_2\text{-H}$), other protons appears as a multiplet between δ 3.103–4.297. **$^{13}\text{C-NMR}$:** Carbonyl carbon at C_6 (206.77) is not shown in hydroxy compound the new asymmetric carbon atom is generated.

DDA $^1\text{H-NMR}$: 7.191–7.418 (10H, m, phenyl protons), 4.305 (2H, s, $\text{N-CH}_2\text{-N}$), 3.808–3.907 (8H, m, N-CH_2 at C_4 , C_8 , C_9 and C_{10}), protons at C_4 , C_8 , C_9 , and C_{10} appeared as double doublet with coupling constant value of $J = 0.031$ Hz. **$^{13}\text{C-NMR}$:** 206.77 (carbonyl carbon at C_6), 137.61, 128.35 and 126.67 (aromatic carbons), 73.06 (C_5 and C_7), 64.40 (C_4 , C_8 , C_9 and C_{10}), 52.75 (NCH_2N at C_2). The molecular structure of the compound is presented in Fig. 1.

Electrochemical studies

Two electrochemical techniques, namely Tafel polarization and EIS, were used to study the corrosion behavior. All electrochemical measurements were carried out using a CHI 760D electrochemical impedance analyzer model maintained at room temperature. For these studies, a three-electrode cell assembly with copper metal as the working electrode, a saturated calomel electrode as the reference electrode, and platinum foil as the counter electrode was used. The working metal specimen (purity 99.9 %) used for electrochemical measurements was covered with epoxy resin, so that its cross-sectional area was 1 cm^2 . Copper specimens were polished using different grades of emery papers (1/0, 2/0, 3/0, 4/0, 5/0, and 6/0). The specimens were washed thoroughly with double-distilled water and finally degreased with acetone and dried at room temperature. The aggressive solution of 1 M HNO_3 was prepared by dilution of analytical grade nitric acid (69 %) with double-distilled water and all electrochemical measurements were carried out in 100-ml unstirred solutions. Before starting the electrochemical experiments, the test sample was stood for 30 min, until steady state was obtained. Impedance measurements were carried out in the frequency range from 0.01 to 1,000 Hz using qn amplitude of 0.005 V peak to peak with an AC signal at the open-circuit potential. The impedance diagrams were plotted in the Nyquist and Bode representations. The Tafel plots were recorded by changing the electrode potential automatically from -300 to 300 mV versus the open-circuit potential at a scan rate of 0.1 mV s^{-1} .

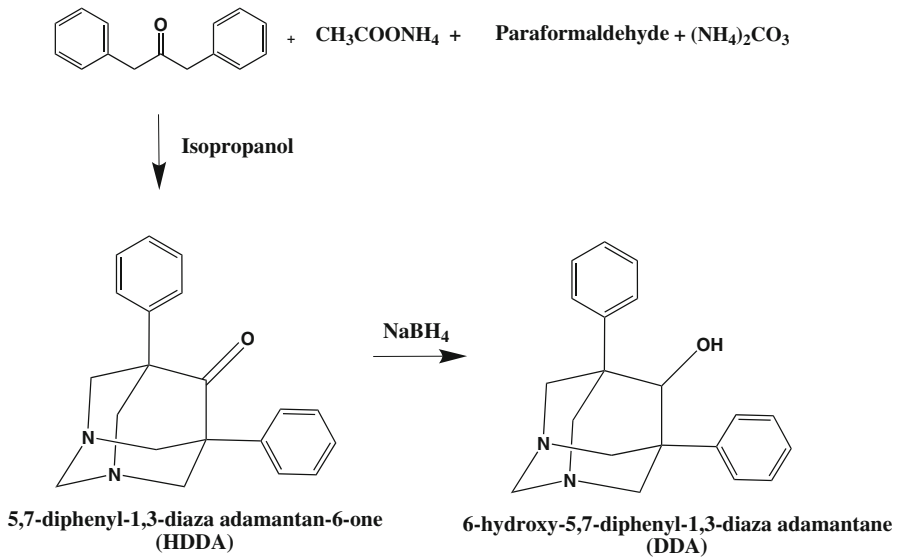


Fig. 1 Synthetic scheme of HDDA and DDA

Weight loss studies

Copper specimens of $3.5 \times 1.0 \times 0.2$ cm were cut with a small hole, 2 mm diameter, at the upper edge of the specimen, used for weight loss studies. The copper samples were polished as mentioned above and a clean weighed copper specimen was completely immersed at an inclined position in a 100-ml beaker. After 3 h of immersion, the sample was withdrawn, rinsed with double-distilled water, washed with acetone, dried and weighed. The weight loss was used to calculate the corrosion rate (W) by the following relationship:

$$W = \frac{m_1 - m_2}{St} \quad (5)$$

where m_1 is the mass of the specimen before corrosion, m_2 is the mass of the specimen after corrosion, S is the total area of the specimen, t is the immersion time in hours, and W is the corrosion rate. The (IE %) was determined by using the following equation;

$$\text{IE \%} = \left[\frac{W_o - W_i}{W_o} \right] \times 100 \quad (6)$$

where W_o is the corrosion rate in the absence of an inhibitor and W_i is the corrosion rate in the presence of inhibitors.

Surface morphology

The copper surface was examined by making photographs of the surface in the absence and presence of optimum concentration of inhibitor (300 ppm) separately

for 3 h. The scanning electron microscopy (SEM) VEGA3TESCAN model and atomic force microscopy (AFM) NTMDT model were used for this purpose. The photographs were taken from that portion of the specimen where better information was expected.

Computational details

All geometry optimizations and quantum chemical calculations were performed using density functional theory (DFT) and utilizing the 6–31+G (d,p) basis sets. DFT/B3LYP is recommended for the study of chemical reactivity and selectivity in terms of the frontier molecular orbital theory [23].

Results and discussion

Electrochemical impedance spectroscopy

The impedance method provides information about the corrosion inhibition process. The kinetics of the electrode processes and the surface properties of the systems were also investigated by this method. Prior to the electrochemical measurement, a stabilization period of 30 min was allowed, which proved to be sufficient to attain stable values of open circuit potential (OCP), which are shown in Fig. 2a, b. Nyquist plots of copper in 1 M HNO₃ solution and corresponding equivalent circuits in the absence and presence of different concentrations of HDDA and DDA are presented in Fig. 3a–c. The impedance spectra exhibit a single semicircle and the diameter of semicircle increases with increase in inhibitor concentrations. The Nyquist plots do not present perfect semi-circles (non-ideal); they show a depressed capacitive loop. These deviations from the perfect circular shape, often known as frequency dispersion, was attributed to surface roughness and inhomogeneities of the solid surface [24–26]. Two different equivalent circuit models were used to give a more accurate fit for both inhibited and uninhibited copper surfaces in 1 M HNO₃ solution. In the equivalent circuit model, R_s represents the solution resistance between the working and reference electrodes and R_{ct} is the charge transfer resistance, which corresponds to the resistance between the metal and outer Helmholtz plane [27–29]. Here, CPE is substituted for the double-layer capacitance to give a more accurate fit. The admittance of CPE is described as

$$Y_{CPE} = Y_o (j\omega)^n \quad (7)$$

where j is the imaginary root, ω the angular frequency, Y_o the magnitude, and n the exponential term [30]. In the Bode plot (Fig. 4), the phase angle at high frequencies provides a general idea of anti-corrosion performance. The more negative the phase angle, the more capacitive the electrochemical behavior [31]. As can be seen from Table 1, R_{ct}^i values increased with increasing the concentration of the inhibitors, indicating a charge transfer process mainly controlling the corrosion of the copper. The charge transfer resistance increment could raise the current tendency to pass through the capacitor in the circuit. According to the appearance of phase angles

versus frequency diagrams, increasing the concentration of HDDA and DDA in the test solutions results in more negative values of the phase angle at high frequencies, indicating superior inhibitive behavior at higher concentrations. This result could be attributed to higher corrosion activity at low concentrations of inhibitors [32]. To obtain the double-layer capacitance (C_{dl}), the frequency at which the imaginary component of the impedance is maximum ($-Z''_{max}$) was discovered and the C_{dl} values were obtained from the following equation:

$$f(-Z''_{max}) = (2\pi C_{dl} R_{ct})^{-1} \quad (8)$$

On the other hand, the values of C_{dl} (Table 4) decrease when compared to the blank value as the concentration of the inhibitor is increased, which confirms the increased level of adsorption of the inhibitors on the metal surface [33]. The adsorption of inhibitors on the copper surface may be attributed to the formation of a protective layer and this may be due to the hetero atoms such as 'N' and 'O', which are present in the inhibitor molecules. The decrease in C_{dl} values results from a decrease in local dielectric constant and/or increase in the thickness of the electrical double layer. It also indicates the gradual replacement of water molecules by the adsorption of the inhibitor molecules on the metal surface, decreasing the magnitude of metal dissolution [34]. The thickness of this protective layer δ_{inh} was related to C_{dl} by the following equation [35]:

$$\delta_{inh} = \frac{\epsilon_0 \epsilon_r}{C_{dl}} \quad (9)$$

where ϵ_0 is the dielectric constant and ϵ_r is the relative dielectric constant. From Table 1, it can be seen that the R_{ct} values increased and the values of C_{dl} decreased with an increase in HDDA and DDA concentrations. This situation was the result of an increase in the surface coverage by these inhibitors, which led to an increase in the inhibition efficiency. R_{ct} values were used to calculate the IE % and surface coverage (θ) according to the following expressions:

$$IE (\%) = \left[\frac{R_{ct}^i - R_{ct}^o}{R_{ct}^i} \right] \times 100 \quad (10)$$

$$\theta = \left[\frac{R_{ct}^i - R_{ct}^o}{R_{ct}^i} \right] \quad (11)$$

where R_{ct}^i and R_{ct}^o are the charge transfer resistance values with and without inhibitors, respectively. Table 1 confirms that the IE % increases with the concentration of inhibitors and the maximum efficiency [88.92 (HDDA) and 87.66 % (DDA)] reaches at 300 ppm. As inhibitor concentration increases, it covers more and more surface area and results in the reduction of the corrosion rate. All the above results infer that, with the increase in inhibitor concentration, the protective film is more protective in HDDA compared to DDA.

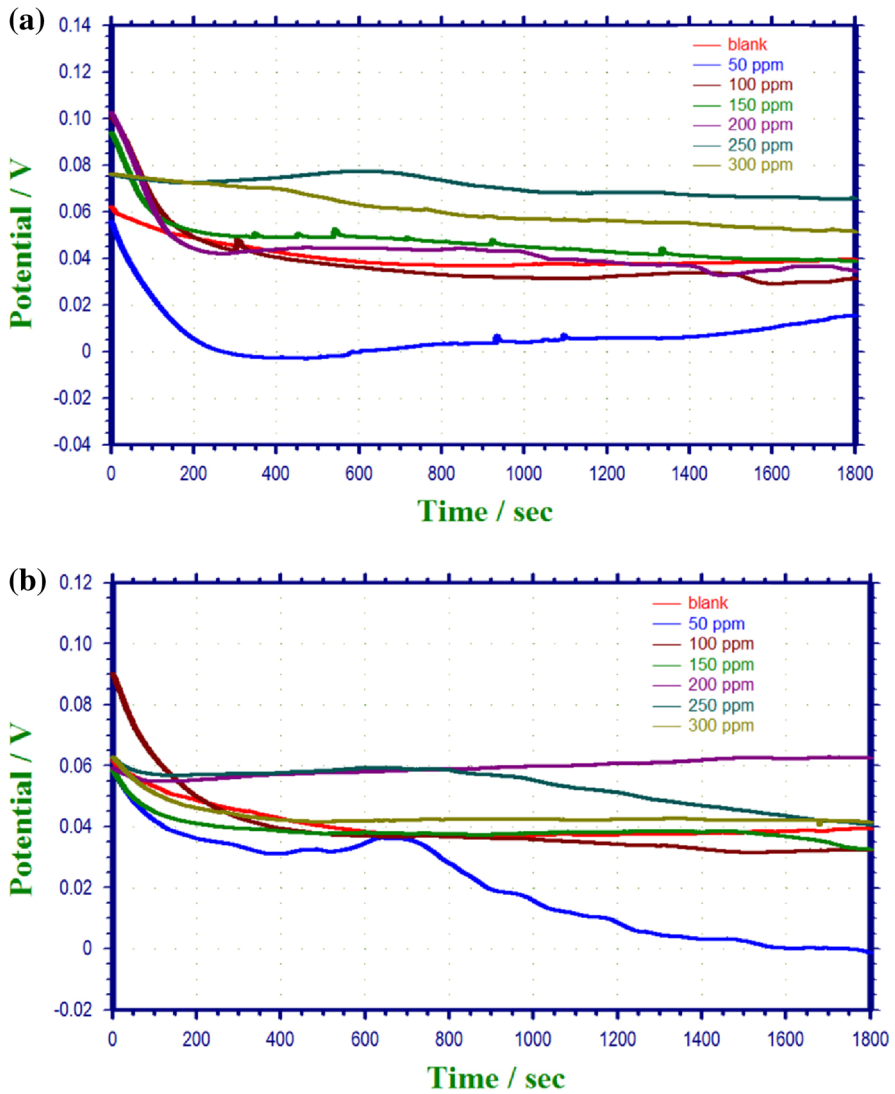
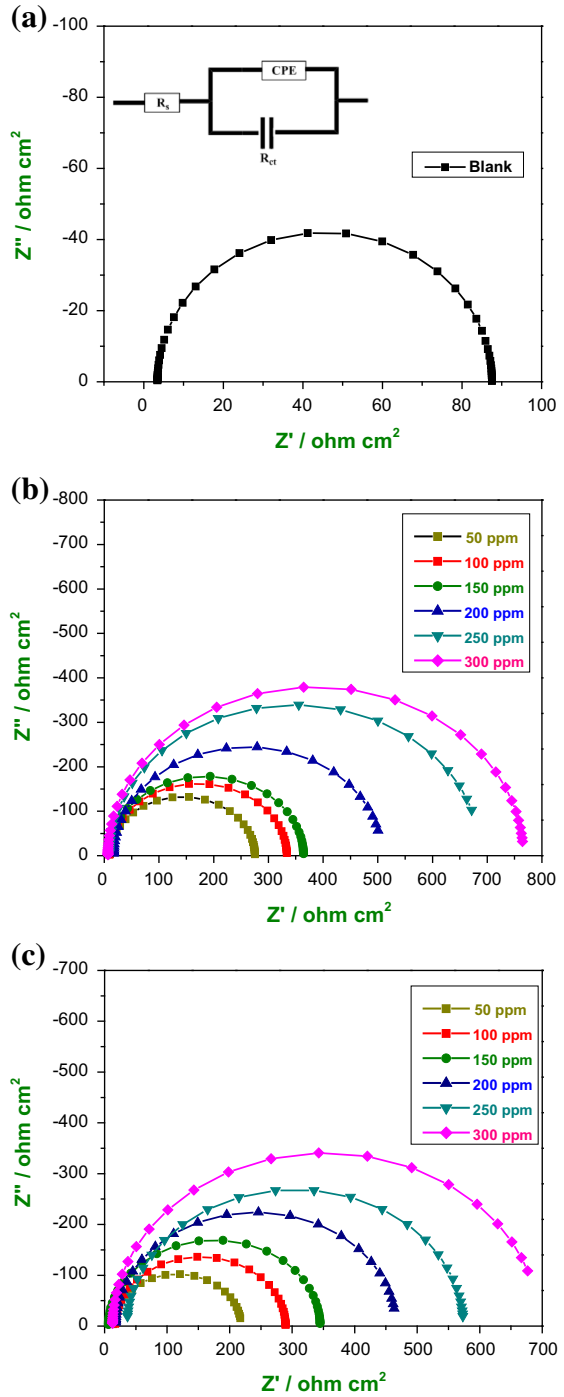


Fig. 2 Open circuit potential for copper in the absence and presence of different concentrations of **a** HDDA, **b** DDA

Tafel polarization

The values obtained from polarization measurements such as corrosion potential (E_{corr}), corrosion current (I_{corr}), anodic and cathodic Tafel slopes (β_a and β_c) are given in Table 2. Inhibition efficiency (IE %) and surface coverage (θ) values were calculated from the relationships:

Fig. 3 Nyquist plots of copper in 1 M HNO₃ solutions with respective electrical circuit models at room temperature: **a** blank, **b** various concentrations of HDDA, **c** various concentrations of DDA



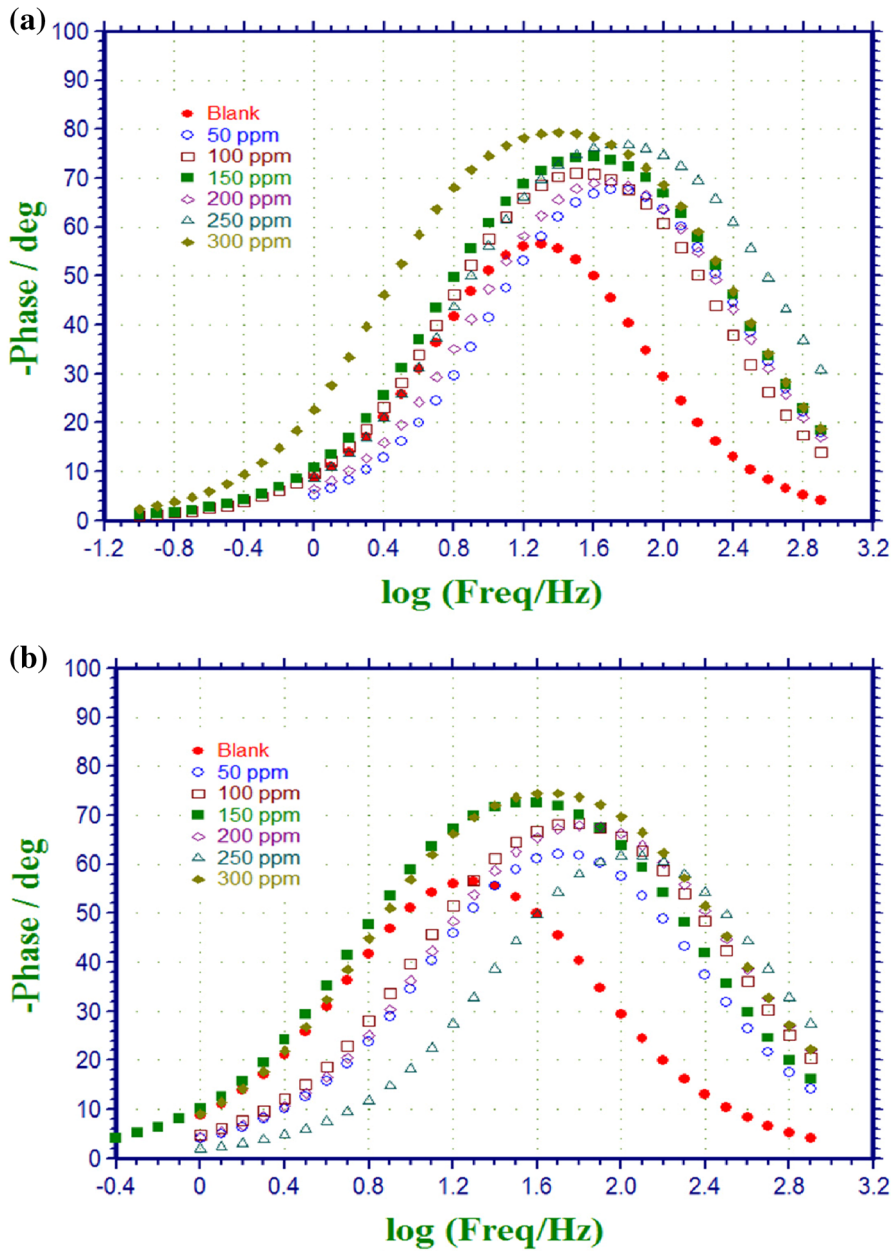


Fig. 4 Bode plots for copper in the presence of different concentrations of **a** HDDA **b** DDA

Table 1 Electrochemical impedance parameters for copper in 1 M HNO₃ containing various concentrations of HDDA and DDA

Concentration of Inhibitor (ppm)	HDDA				DDA			
	R_{ct} ($\Omega \text{ cm}^2$)	C_{dl} ($\mu\text{F cm}^{-2}$)	Surface coverage (Θ)	IE η (%)	R_{ct} ($\Omega \text{ cm}^2$)	C_{dl} ($\mu\text{F cm}^{-2}$)	Surface coverage (Θ)	IE η (%)
Blank	84.291	36.897	–	–	84.291	36.897	–	–
50	275.42	4.295	0.6940	69.3955	204.66	6.3934	0.5881	58.8141
100	325.11	3.038	0.7407	74.0731	272.81	4.2877	0.6910	69.1027
150	357.39	2.492	0.7641	76.4148	338.82	2.7493	0.7512	75.1222
200	489.04	1.322	0.8276	82.7640	448.17	1.5762	0.8119	81.1922
250	678.98	0.692	0.8759	87.5856	537.46	1.1003	0.8432	84.3168
300	760.41	0.552	0.8892	88.9151	683.16	0.6686	0.8766	87.6616

$$\text{IE (\%)} = \left[\frac{I_{\text{corr}}^o - I_{\text{corr}}^i}{I_{\text{corr}}^o} \right] \times 100 \quad (12)$$

$$\theta = \left[\frac{I_{\text{corr}}^o - I_{\text{corr}}^i}{I_{\text{corr}}^o} \right] \quad (13)$$

where I_{corr}^o and I_{corr}^i are the corrosion current densities in the absence and presence of the inhibitor, respectively. The polarization results are also in conformation with the impedance results. In Table 2, it is shown that the polarization curves in Fig. 5a–c exhibit no steep slope in the anodic range, meaning that no passive films are formed on the copper surface. Consequently, copper may directly dissolve in 1 M HNO₃ solutions. From Fig. 5a–c, it is clear that both the cathodic and anodic reactions are inhibited and the inhibition increases as the inhibitor concentration increases, but the cathodic Tafel slope is shifted to a great extent on the copper surface while the shift in anodic slope is less. For example, in the presence of 300 ppm HDDA and DDA, the cathodic Tafel slope (β_c) is shifted from 482.16 to 300.93 and 318.47 mV dec⁻¹ on the copper surface, whereas the anodic slope is shifted from 109.83 to 74.29 and 83.51 mV dec⁻¹. The same is true at all the concentrations of the corrosive environment. It may be inferred that all the inhibitors on the copper surface predominantly control the cathodic reaction of the corrosion process and thus protect the copper from corrosion. Similar results were also observed in Bianmei et al., Khalad, and Appa Rao et al. [36–38]. This indicated that the corrosion products prevent corrosion by depositing on the copper surface and blocking the mass transportation of the corrosion process [39]. It is also well known from quantum chemical calculations that HDDA and DDA have nitrogen and oxygen atoms with a lone pair of electrons which may easily adsorb on the metal surface. From Table 2, it is clear that there was no definite trend in the shift of E_{corr} values in the presence of various concentrations of adamantane derivatives in the 1-M HNO₃ solution. This result indicated that adamantane derivatives can be classified as a mixed-type inhibitor in 1 M HNO₃ solution. The values of the corrosion current density (I_{corr}) for copper corrosion reactions without and with

inhibitors were determined by extrapolation of the cathodic and anodic Tafel lines to the corrosion potential (E_{corr}). It is obvious from Fig. 5a, b that the Tafel curves are shifted to lower corrosion current densities as the inhibitor concentration is raised. The I_{corr} values decrease steadily from the blank value with the increase in inhibitor concentration from 50 to 300 ppm. This decrease in I_{corr} is an indication of a decrease in corrosion reaction, since the corrosion current is proportional to the magnitude of the corrosion reaction. The decrease in I_{corr} clearly confirms that the inhibition efficiency increases with the concentrations of adamantane derivatives. It was also found that the R_p value increases with increasing inhibitor concentration, which suggests the retardation of copper corrosion in inhibited solutions compared to uninhibited ones.

HDDA and DDA attained maximum inhibition efficiency from the Tafel polarization at 300 ppm concentrations of 88.61 and 85.23 %, respectively, and these are correlated with EIS measurements. The results listed in Table 2 reveal that HDDA is the more effective corrosion inhibitor in comparison to DDA.

Weight loss studies

The values of percentage inhibition efficiency (IE %) and corrosion rate (W) obtained from the weight loss method at different concentrations (50–300 ppm) and various temperatures are summarized in Table 3. It is observed from Fig. 6c that the IE % of both HDDA and DDA increases with increasing the inhibitor concentration in 1 M HNO_3 and shows a sharp increase in the inhibition, which reached its maximum value at a concentration of 300 ppm, while a further increase in the inhibitor concentration does not show any appreciable change in the inhibition efficiency. The reason for this may be that all active sites of the copper surface are occupied by the inhibitor molecules and no vacant sites are available for further adsorption.

The inhibitory behavior of the compounds against copper corrosion can be attributed to the adsorption of inhibitors on the copper surface, which limits the dissolution of the metal by blocking its corrosion sites and hence decreasing the corrosion rate (W) from 28.87 to 2.64 and 3.62 $\text{mg cm}^{-2} \text{h}^{-1}$ for HDDA and DDA, respectively. W decreases with increasing IE % from 50 to 300 ppm inhibitor concentration. It is clear that both HDDA and DDA showed good inhibition for copper corrosion in the 1-M HNO_3 solution because the inhibitor molecules have two benzene rings and N, O atoms as active centers. The inhibitor compound can be adsorbed by the interaction between the lone pairs of electrons of the nitrogen and oxygen atoms with the copper surface.

Figure 6a, b also shows that, with the increase in temperature, the IE % initially decreases slightly from 303 to 313 K and then suddenly decreases with further increases in temperature. The decrease of IE % with temperature may be attributed to desorption of the inhibitor molecules of metal surfaces at higher temperatures [40].

It is worth noting from Tables 1, 2 and 3 that the IE % values obtained from the weight loss and electrochemical measurements are comparable and run parallel with each other. The small difference found in the results obtained from both chemical and electrochemical measurements have been reported previously [41]. The authors attributed this difference between electrochemically and chemically determined

Table 2 Tafel polarization values for the corrosion of copper in 1 M HNO₃ containing various concentrations of HDDA and DDA

Concentration of Inhibitor (ppm)	b_a (mV dec ⁻¹)	b_c (mV dec ⁻¹)	E_{corr} (mV/SCE)	I_{corr} (mA cm ⁻²)	Linear polarization (Ω)	Surface coverage (Θ)	I.E (%)
HDDA							
Blank	109.83	482.16	40.8	1.358	29	–	–
50	102.17	725.69	22.3	0.6614	59	0.513	51.296
100	91.10	337.84	39.6	0.5185	60	0.6182	61.8189
150	79.61	351.49	37.3	0.3266	86	0.7595	75.95
200	69.40	755.29	77.1	0.2485	111	0.817	81.701
250	73.37	367.11	69.4	0.2186	122	0.839	83.9028
300	74.29	300.93	45.2	0.1547	168	0.8861	88.6082
DDA							
50	99.2	535.62	39.4	0.7201	51	0.4697	46.9735
100	112.78	475.96	26.2	0.5445	73	0.599	59.9043
150	83.27	345.54	40.8	0.3744	78	0.7243	72.43
200	96.43	278.47	34.9	0.3273	95	0.759	75.8984
250	77.89	290.78	36.4	0.274	98	0.7982	79.8233
300	83.51	318.47	25.8	0.2006	144	0.8523	85.2283

corrosion rates to the operation of a separate potential, independent of the chemical dissolution process which co-exists with the electrochemical process.

Adsorption isotherm

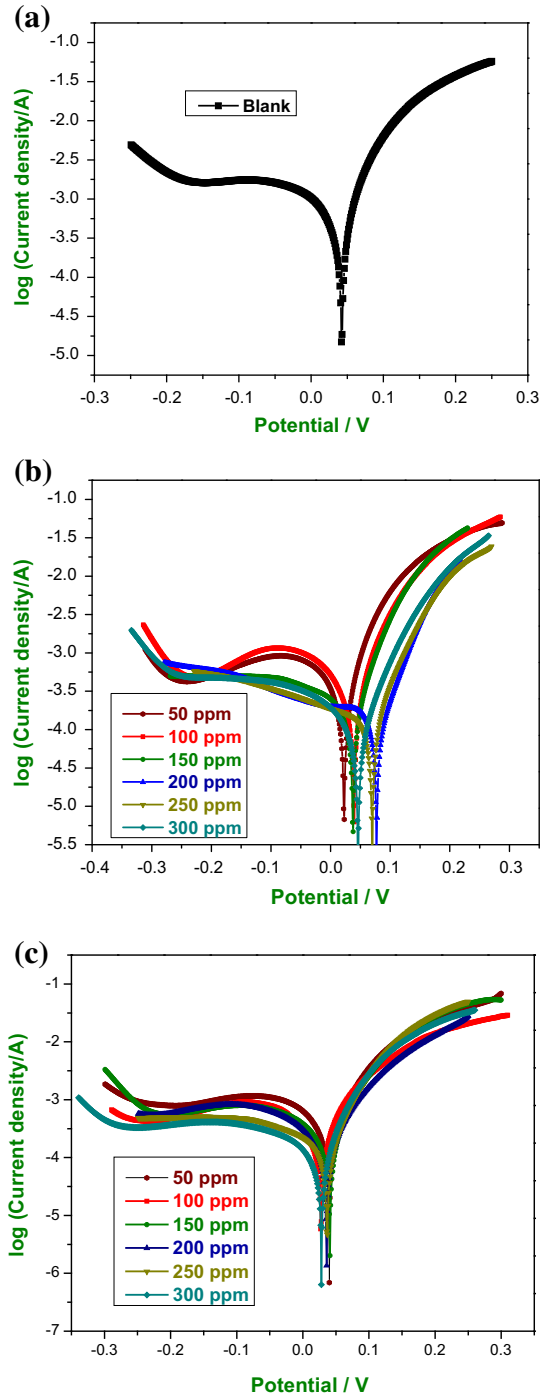
It is widely acknowledged that adsorption isotherms provide useful insights into the mechanism of corrosion inhibition. The adsorption isotherm study describes the interaction between inhibitor molecules and copper surface. For this purpose, the values of surface coverage (θ) at different concentrations of inhibitor in 1 M HNO₃ medium were calculated. The most frequently used adsorption isotherms are Frumkin, Temkin and Langmuir isotherms. Attempts to fit data obtained from the weight loss measurements into different adsorption isotherms revealed that the data best fitted to the Langmuir adsorption isotherm. Assumptions of Langmuir relate the concentration of the adsorbate in the bulk of the electrolyte (C_{inh}) to the degree of surface coverage (θ) as in Eq. (14):

$$\frac{C_{\text{inh}}}{\theta} = \frac{1}{K_{\text{ads}}} + C_{\text{inh}} \quad (14)$$

where K_{ads} is the equilibrium constant of adsorption. Figure 7a, b shows the relationship between C_{inh}/θ and C_{inh} for optimum concentration of inhibitor which gives a straight line.

This result shows that the regression coefficient (R^2) is almost equal to unity and the slope is very close to unity. This indicates that the adsorption of inhibitors

Fig. 5 Anodic and cathodic Tafel polarization plots of copper in 1 M HNO₃ solution with various concentrations of inhibitors: **a** blank, **b** HDDA, **c** DDA



follows the Langmuir adsorption isotherm. The slope of the C_{inh}/θ versus C_{inh} plots shows a deviation from unity, which means non-ideal simulating and is unexpected from the Langmuir adsorption isotherm [42]. It might be the result of the interactions between the adsorbed species on the copper surface. The adsorption equilibrium constant (K_{ads}) and free energy of adsorption ($\Delta G_{\text{ads}}^{\circ}$) were calculated and are listed in Table 4 using the following relationship (15):

$$\Delta G_{\text{ads}}^{\circ} = -RT \ln(55.5 K_{\text{ads}}) \quad (15)$$

where 55.5 is the concentration of water in solution in mol L^{-1} and R is the universal gas constant. The adsorption is influenced by the nature and charge of the metal, the chemical structure of inhibitor and the type of aggressive electrolyte. Therefore, the value of E_{corr} in the nitric acid solution is positive, so the copper surface acquires a positive charge. Accordingly, nitrate ions are first adsorbed on the metal surface and consequently the copper surface becomes negatively charged. The adamantane derivatives contained a bicyclic ring with electron-donating polar atoms such as N and O atoms. In acidic solutions, this compound could be protonated easily on the copper surface:



Generally, the values of $\Delta G_{\text{ads}}^{\circ}$ around -20 kJ mol^{-1} or lower are consistent with the electrostatic interaction, and, when it is around -40 kJ mol^{-1} or higher values, then this is a chemical interaction [43]. Here, the calculated $\Delta G_{\text{ads}}^{\circ}$ values are below $-17.73 \text{ kJ mol}^{-1}$, which indicates that the protonated adamantane derivatives are adsorbed on the copper surface solely by physical adsorption (electrostatic interaction).

Theoretical calculation

The calculated quantum chemical parameters necessary for discussion of the reactivity of the selected are reported in Table 5. The HOMO and the LUMO orbitals of the studied adamantane derivatives are also shown in Fig. 8a–d. The HOMO is delocalized throughout the inhibitor molecules except on the two benzene rings. These results suggest that the phenyl rings have a smaller tendency to donate electrons. The LUMO is also delocalized in certain regions of the molecules: in structure HDDA, the LUMO is strongly delocalized in the hydroxy group; in structure DDA, the LUMO is delocalized on the keto group. The energy of the HOMO (E_{HOMO}) represents the ability of the molecule to donate a lone pair of electrons, and the higher the E_{HOMO} value, the greater the tendency of the molecule to donate electrons to an electrophilic reagent [44]. The results show that E_{HOMO} follows the order HDDA > DDA. E_{LUMO} represent the ability of the molecule to accept electrons from a donor reagent, and the lower the E_{LUMO} , the greater the tendency of the molecule to accept electrons. Results from Table 5 show that E_{LUMO} decreases in the order HDDA < DDA. The energy difference between E_{HOMO} and E_{LUMO} (i.e. ΔE) informs on the reactivity of the given compound: the smaller the ΔE value, the greater the reactivity of the molecule. The results show

Table 3 Corrosion parameters obtained from weight loss measurements for copper in 1 M HNO₃ containing various concentrations of diaza-adamantane derivatives at different temperatures

Concentration of inhibitor (ppm)	Weight loss (mg)			Corrosion rate (mg cm ⁻² h ⁻¹)			Inhibition efficiency (%)					
	303 K	308 K	318 K	328 K	303 K	308 K	318 K	328 K	303 K	308 K	318 K	328 K
HDDA												
Blank	11.26	11.98	13.44	14.81	28.87	30.71	34.46	37.97	—	—	—	—
50	5.19	5.90	8.01	9.24	13.31	15.13	20.54	23.69	53.90	50.73	40.39	37.61
100	4.32	5.06	7.24	8.66	11.08	12.97	18.56	22.21	61.62	57.71	46.14	41.51
150	3.16	4.10	6.21	7.80	8.10	10.51	5.92	20.00	71.94	65.78	53.80	47.33
200	2.21	3.23	5.57	6.76	5.67	8.28	14.28	17.33	80.36	73.04	58.56	54.36
250	1.790	2.40	4.31	5.43	4.59	6.15	11.05	13.92	84.10	79.98	67.93	63.34
300	1.03	1.68	3.28	4.84	2.64	4.10	8.41	12.41	90.86	86.65	75.59	67.32
DDA												
Blank	11.26	11.98	13.44	14.81	28.87	30.71	34.46	37.97	—	—	—	—
50	5.00	5.97	8.41	9.09	12.82	15.31	21.56	23.31	55.60	50.15	37.43	38.61
100	4.36	5.02	7.11	8.71	11.18	12.87	18.23	22.33	61.27	58.09	47.10	41.19
150	3.28	4.38	6.43	7.69	8.41	11.08	16.49	19.72	70.87	63.92	52.15	48.06
200	2.40	3.44	6.02	6.90	6.15	8.82	15.44	17.69	78.70	71.28	55.19	53.41
250	1.88	2.74	5.11	5.66	4.82	7.03	13.10	14.51	83.30	77.11	61.98	61.79
300	1.41	1.96	3.80	4.90	3.62	5.03	9.74	12.56	87.46	83.62	71.74	66.92

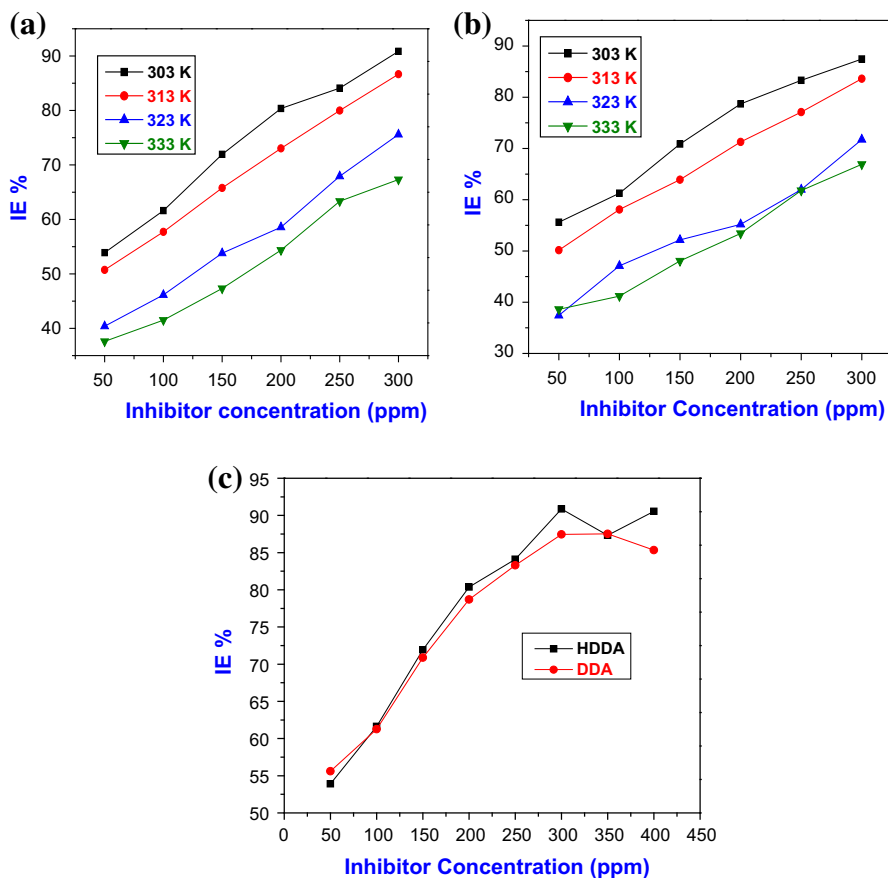


Fig. 6 Variations of IE % in 1 M HNO₃ on the copper surface at **a** various concentrations of HDDA at different temperatures and **b** various concentrations of DDA at different temperatures; **c** a comparison of inhibition efficiencies with different concentrations of inhibitors at room temperature

that HDDA has a smaller ΔE value (4.362 eV) than DDA (4.8809 eV), and is therefore the most reactive molecule. In this way, HDDA would readily adsorb on the metal surface resulting in higher inhibition efficiency.

The dipole moment gives information on the polarity (the hydrophobicity) of a molecule and therefore the electron distribution in the molecule. The higher the dipole moment, the higher the polarity of the molecule. In the study of corrosion inhibition, two different trends are often seen, correlating dipole moment with the IE %; inhibition efficiency has been reported to increase with the increase in the dipole moment of the inhibitor [45], while in other reports, inhibition efficiency has been reported to increase with the decrease in the dipole moment of the inhibitor [46]. In the current work, the order of inhibition efficiency is such that DDA < HDDA, which implies that inhibition efficiency increases with the decrease in the dipole moment of the molecules.

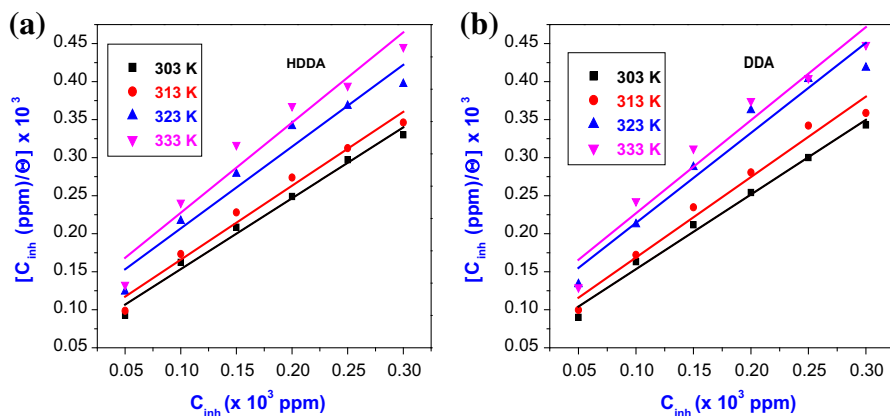


Fig. 7 Langmuir adsorption isotherm plots of copper surface in 1 M HNO₃ solutions at various temperatures: **a** various concentrations of HDDA, **b** various concentrations of DDA

Table 4 Langmuir adsorption isotherm parameters for diaza-adamantane derivatives in 1 M HNO₃ on the copper metal at different temperatures

Temperature (K)	HDDA			DDA		
	R^2	K_{ads} (10^4 M^{-1})	$\Delta G_{\text{ads}}^{\circ}$ (KJ mol^{-1})	R^2	K_{ads} (10^4 M^{-1})	$\Delta G_{\text{ads}}^{\circ}$ (KJ mol^{-1})
303	0.9850	15.51	-17.02	0.9871	17.81	-17.37
313	0.9733	14.18	-17.35	0.9710	16.82	-17.80
323	0.9379	10.82	-17.18	0.9461	12.35	-17.54
333	0.9367	10.89	-17.73	0.9391	11.72	-17.93

The HOMO and LUMO diagrams (Fig. 8a–d) reflect that the orbital electron densities were distributed homogeneously throughout the molecules. Therefore, the more negative the Mulliken atomic charges of the adsorbed inhibitors, the more easily the atom donates its electrons to the unoccupied orbital of the metal, and adsorbs preferentially on the metal surface with the formation of a closely packed adsorption layer to inhibit copper ions from entering the solution. It is clear from HDDA and DDA that nitrogen and oxygen atoms carrying more negative charges could offer electrons to the metal surface to form a protective film, while oxygen atoms in HDDA have a more negative charge (-0.611 eV) than ketonic oxygen in DDA (-0.409 eV). In the current study, the reactivity of the molecules has been found to follow the order HDDA > DDA, which is also in agreement with the experimentally determined inhibition efficiency IE %.

Table 5 Quantum chemical parameters of diaza-adamantane derivatives

Inhibitor	E_{HOMO} (eV)	E_{LUMO} (eV)	μ (D)	$\Delta E = (E_{\text{HOMO}} - E_{\text{LUMO}})$ (eV)	Total energy (A.U)	I.E (%) ^a
HDDA	-5.2905	-0.9285	2.7147	4.3620	-956.17	90.84
DDA	-5.6135	-0.7325	1.9029	4.8809	-958.62	89.87

^a I.E (%) values were calculated from Tafel polarization measurements

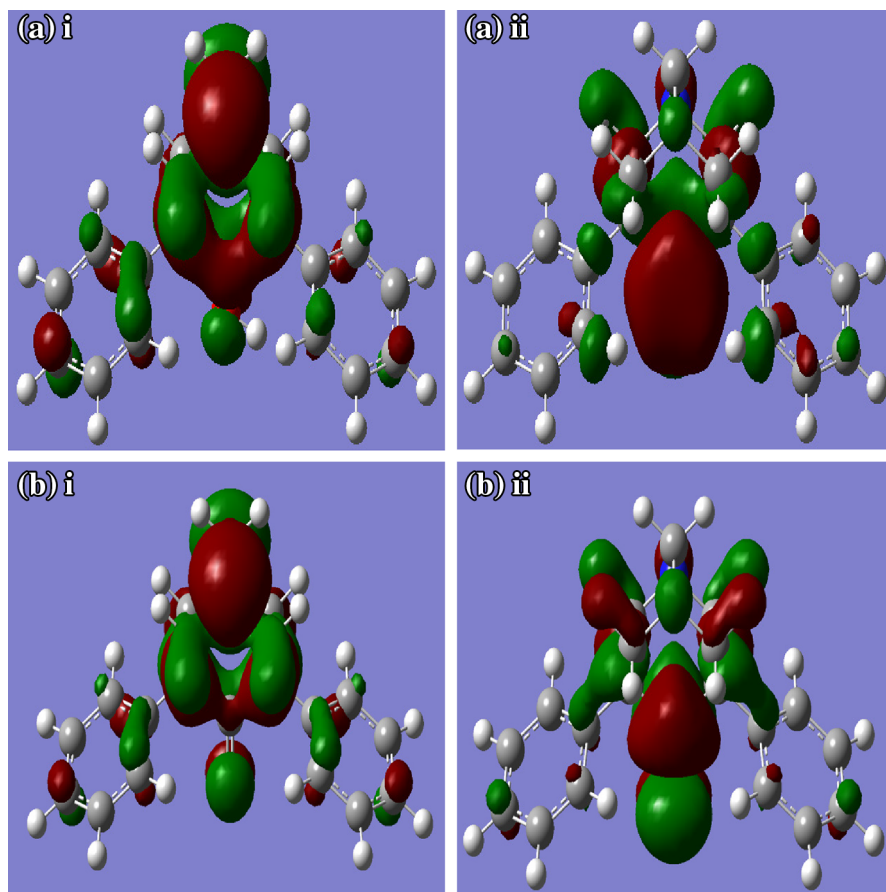


Fig. 8 The frontier molecular orbital density distribution of diaza-adamantane derivatives **a** HDDA (*left*, HOMO; *right*, LUMO) and **b** DDA (*left*, HOMO; *right*, LUMO)

Surface studies

Scanning electron microscopy (SEM)

The SEM images were recorded (Fig. 9a–d) to establish the interaction of inhibitor molecules with metal surface. The SEM images show the features of

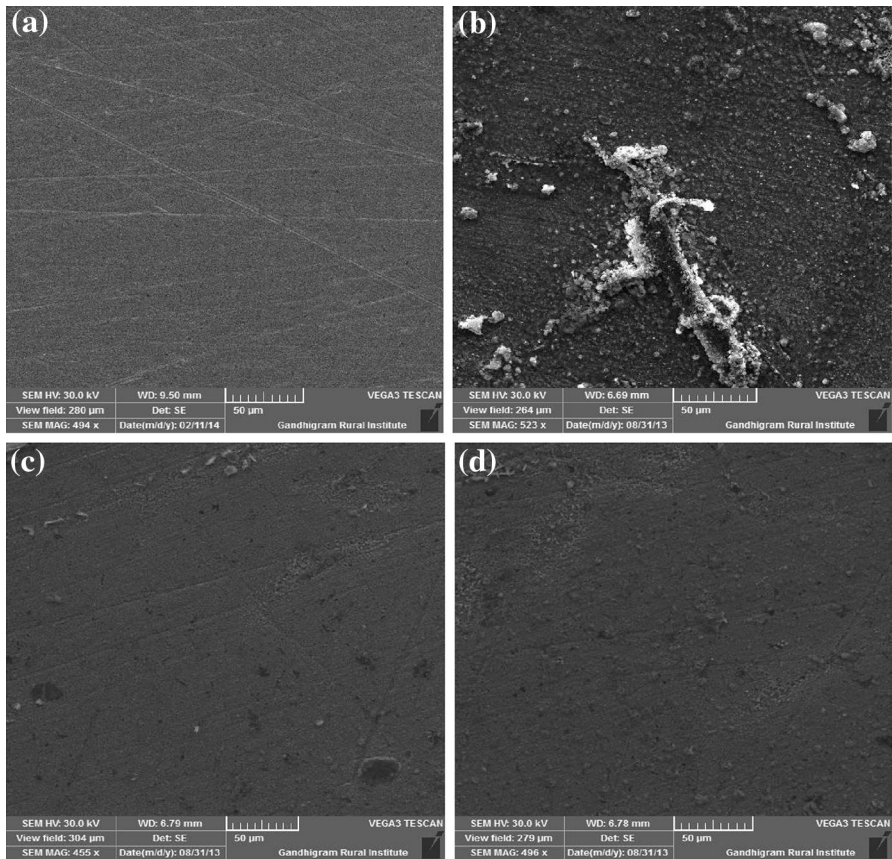


Fig. 9 SEM micrographs of surface of copper after 3 h of immersion in 1 M HNO_3 solution: **a** polished surface, **b** blank surface, **c** HDDA, **d** DDA

copper surface after 3 h in 1 M HNO_3 in the absence and presence of 300 ppm HDDA and DDA. Figure 9a shows the polished surface of copper, so that a comparison can be drawn with the morphology after exposure to the 1 M HNO_3 solution (blank) shown in Fig. 9b. In Fig. 9a, the polished copper surface shows some fine scratches obtained during the grinding procedure [47]. Inspection of Fig. 9b reveals that there is severe damage and corrosion products formed on the surface of copper. Figure 9c, d shows that there are fewer pits and cracks observed in the inhibited surface and that it is in better condition having a smooth surface while the metal surface immersed in blank acid solutions is rough. This clearly indicates that the corrosion of copper decreased remarkably in the presence of HDDA and DDA, and that the copper surfaces are fully covered by the inhibitor molecules and a protective film was formed.

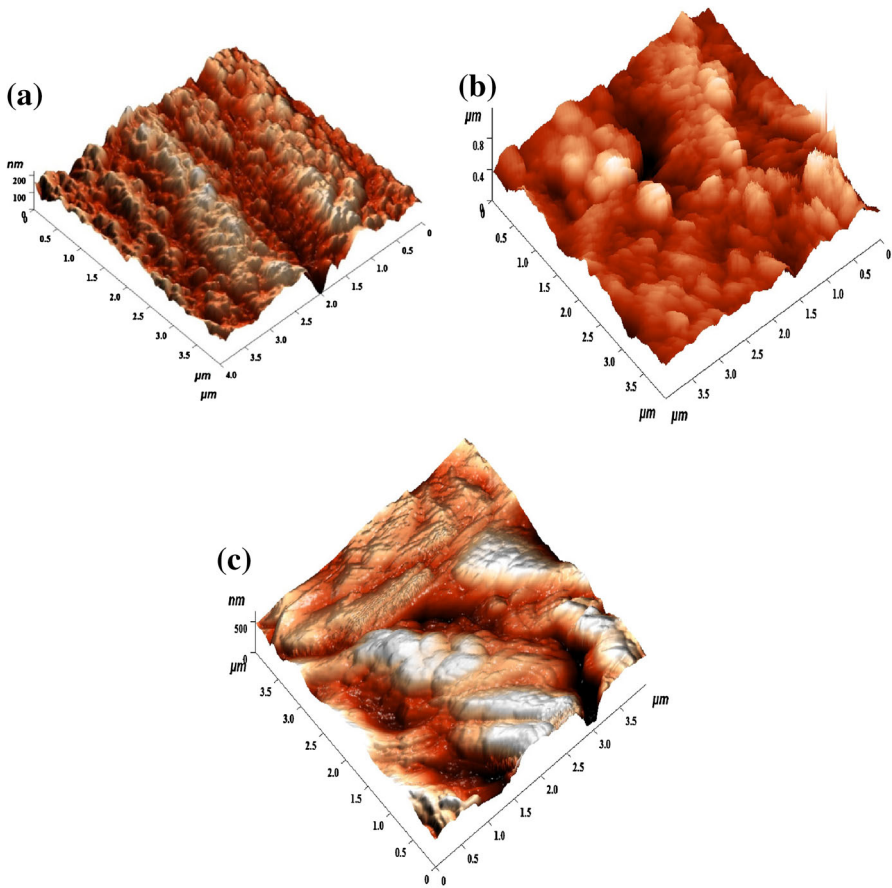


Fig. 10 AFM images of copper surface immersed in 1 M HNO_3 with and without 300 ppm concentration: **a** blank, **b** HDDA, **c** DDA

Atomic force microscopy (AFM)

AFM is a powerful technique to investigate the surface morphology at nano- to micro-scale and has become a new choice to study the influence of inhibitors on the generation and the progress of the corrosion of the metal/solution interface. The three-dimensional AFM morphologies for the copper surface immersed in 1 M HNO_3 with and without 300 ppm HDDA and DDA are shown in Fig. 10a–c. The root mean square (rms) and average roughness values were carried out for both the protected and unprotected copper surfaces are given in Table 6. The rms roughness and maximum peak-to-peak height data suggests that the copper surface immersed in 1 M HNO_3 has a greater surface roughness than the protected metal surface. The presence of HDDA and DDA in 1 M HNO_3 significantly reduced to 53.5694 and 59.0195 nm, respectively, when compared with the 307.145 nm of the copper metal surface immersed in 1 M HNO_3 . These parameters confirm that the surface appears

Table 6 AFM data for the copper surface immersed in 1 M HNO₃ with and without 300 ppm HDDA and DDA

Samples	Root mean square roughness (nm)	Maximum peak-to-peak height (nm)	Ten point height (nm)	Average roughness (nm)
Polished surface	32.1001	227.883	114.552	25.8304
1 M HNO ₃	406.869	2,448.1	1,227.86	307.145
HDDA	78.6873	606.06	303.907	59.0195
DDA	73.014	686.803	344.346	53.9654

smoother, and that the smoothness is due to the formation of a compact protective film of HDDA and DDA on the metal surface, thereby inhibiting the corrosion of the copper metal. A uniform variation of the thickness in section analysis also indicates homogeneity of the film.

Conclusions

On the basis of the above results, the newly synthesized diaza-adamantane derivatives were found to act as good corrosion inhibitors for copper surfaces in 1 M HNO₃ media. Reasonably good agreement was observed between the values obtained from the weight loss, electrochemical impedance, and Tafel polarization techniques. All the experimental studies show that the HDDA gives a better corrosion inhibition performance than DDA. The adsorption of diaza-adamantane derivatives on the copper surface in 1 M HNO₃ obeys the Langmuir adsorption isotherm. Values of $\Delta G_{\text{ads}}^{\circ}$ indicate that HDDA and DDA are inhibiting the corrosion of copper purely by physisorption. Tafel polarization studies have shown that diaza-adamantane derivatives act as mixed-type inhibitors, but predominantly control the cathodic reaction. The quantum mechanical approach may well be able to foretell molecule structures that are better for corrosion inhibition. The inhibition efficiency increases with the increase in E_{HOMO} and the decrease in E_{LUMO} and dipole moment (μ). The SEM images confirm the formation of a protective layer on the copper surface. AFM studies also show the surface morphology by calculating the roughness of the copper samples and suggesting that the roughness is decreased after the use of these inhibitors.

Acknowledgments All the authors are grateful to the University Grand Commission (UGC) for assistance through basic science research (BSR), special assistance programme (SAP) and major research project (MRP).

References

1. S. Fouda, M.N. Moussa, F.I. Taha, A.I. Elneanaa, *Corros. Sci.* **26**, 719 (1986)
2. R. Solmaz, G. Kardas, B. Yazici, M. Erbil, *Colloids Surf. A* **312**, 7 (2008)
3. B. Joseph, A. Joseph, *Port. Electrochim. Acta* **29**, 253 (2011)

4. P. Morales-Gil, G. Negron-Silva, M. Romero-Romo, C. Angeles-Chavez, M. Palomar-Pardave, *Electrochim. Acta* **49**, 4733 (2004)
5. M.A. Quraishi, R. Sardar, *Mater. Chem. Phys.* **78**, 425 (2003)
6. D.P. Schweinsberg, G.A. George, A.K. Nanayakkara, D.A. Steinert, *Corros. Sci.* **28**, 33 (1988)
7. P.M. Niamien, H.A. Kouassi, A. Trokourey, F.K. Essy, D. Sissouma, Y. Bokra, *ISRN Mater. Sci.* (2012). doi:[10.5402/2012/623754](https://doi.org/10.5402/2012/623754)
8. M. Sherif, S.M. Park, *Electrochim. Acta* **51**, 6556 (2006)
9. E.M. Sherif, R.M. Erasmus, J.D. Comins, *Corros. Sci.* **50**, 3439 (2008)
10. E.M. Sherif, R.M. Erasmus, J.D. Comins, *J. Colloid Interface Sci.* **306**, 96 (2007)
11. A. Zarrouk, B. Hammouti, A. Dafali, F. Bentiss, *Ind. Eng. Chem. Res.* **52**, 2560 (2013)
12. P.M. Niamien, F.K. Essy, A. Trokourey, D. Sissouma, D. Diabate, *Afr. J. Environ. Sci. Technol.* **5**, 641 (2011)
13. Olusegun.K. Abiola, Moriamo.O. John, Patric.O. Asekunowo, Peter.C. Okafor, Oladele.O. James, *Green. Chem. Lett. Rev.* **4**, 273 (2011)
14. A.S. Fouda, M.M. Gouda, S.I. Abdul, El-Rahman. *Bull. Korean Chem. Soc.* **21**, 1085 (2000)
15. A. Zarrouk, H. Zarrok, R. Salghi, B. Hammouti, S.S. Al-Deyab, R. Touzani, M. Bouachrine, I. Warad, T.B. Hadda, *Int. J. Electrochem. Sci.* **7**, 6353 (2012)
16. A. Zarrouk, B. Hammouti, H. Zarrok, R. Salghi, M.F. Bouachrine, S.S. Bentiss, Al-Deyab. *Res. Chem. Intermed.* **38**, 2327 (2012)
17. Da-quan. Zhang, Zhong-xun. An, Qing-yi. Pan, Li-xin. Gao, Guo-ding. Zhou, *Corros. Sci.* **48**, 1437 (2006)
18. M. Singh, R.B. Rastogi, B.N. Upadhyay, *Corrosion* **50**, 620 (1994)
19. K.F. Khaled, M.A. Amin, *J. Appl. Electrochem.* **38**, 1609 (2008)
20. K.F. Khaled, K. Babi-Samardzija, N. Hackerman, *J. Appl. Electrochem.* **34**, 697 (2004)
21. M.A. Quraishi, I. Ahamad, A.K. Singh, S.K. Shukla, B. Lal, V. Singh, *Mat. Chem. Phys.* **112**, 1035 (2008)
22. J. Stetter, K. Schafer, Dieminger. *Chem. Ber.* **91**, 598 (1958)
23. M.K. Kabanda, S.K. Shukla, A.K. Singh, L.C. Murulana, E.E. Ebenso, *Int. J. Electrochem. Sci.* **7**, 8813 (2012)
24. H. Shih, H. Mansfeld, *Corros. Sci.* **29**, 1235 (1989)
25. S. Martinez, M. Mansfeld-Hukovic, *J. Appl. Electrochem.* **33**, 1137 (2003)
26. M. Elayyachy, A. El Idrissi, B. Hammouti, *Corros. Sci.* **48**, 2470 (2006)
27. X.Y. Liu, S.H. Chen, H.Y. Ma, G.Z. Liu, L.X. Shen, *Appl. Surf. Sci.* **253**, 814 (2006)
28. S.M. Behpour, N. Ghoreishi, M. Soltani, Salavati-Niasari. *Corros. Sci.* **51**, 1073 (2009)
29. E. Machnikova, K.H. Whitmire, N. Hackerman, *Electrochim. Acta* **53**, 6024 (2008)
30. J. Zhang, J. Zhao, N. Zhang, C. Qu, X. Zhang, *Ind. Eng. Chem. Res.* **50**, 7264 (2011)
31. M. Mahdavian, M.M. Attar, *Corros. Sci.* **48**, 4152 (2006)
32. M. Mahdavian, S. Ashhari, *Electrochim. Acta* **55**, 1720 (2010)
33. A.V. Shanbhag, T.V. Venkatesha, R.A. Prabhu, R.G. Kalkhambkar, G.M. Kulkarni, *J. Appl. Electrochem.* **38**, 279 (2008)
34. G. Karthik, M. Sundaravadivelu, P. Rajkumar, *Res. Chem. Intermed.* (2013). doi:[10.1007/s11164-013-1291-0](https://doi.org/10.1007/s11164-013-1291-0)
35. H.H. Hassan, *Electrochim. Acta* **51**, 5966 (2006)
36. Bianmei. Cao, Tingfei. Xi, Yudong. Zheng, David. Hui, *Metalurgija-MJoM* **17**, 111 (2011)
37. K.F. Khaled, *Corros. Sci.* **52**, 3225 (2010)
38. B.V. Appa Rao, Md Yakub Iqbal, B. Sreedhar, *Corros. Sci.* **51**, 1441 (2009)
39. C. Bianmei, X. Tingfei, Z. Yudong, *Biomed. Mater.* **3**, 044114 (2008)
40. A. Chetouani, A. Aouniti, B. Hammouti, N. Benchat, T. Benhaddi, S. Kertit, *Corros. Sci.* **45**, 1675 (2003)
41. K.F. Khaled, *Corros. Sci.* **52**, 2905 (2010)
42. M. Lebrini, M. Lagrenee, H. Vezin, M. Traisnal, F. Bentiss, *Corros. Sci.* **49**, 2254 (2007)
43. M.G. Hosseini, M. Ehteshamzadeh, T. Shahrabi, *Electrochim. Acta* **52**, 3680 (2007)
44. A. Fedorov, Y.N. Zhuravlev, V.P. Berveno, *Phys. Chem. Phys.* **13**, 5679 (2011)
45. N.O. Eddy, F.E. Awe, C.E. Gimba, N.O. Ibisi, E.E. Ebenso, *Int. J. Electrochem. Sci.* **6**, 931 (2011)
46. N.O. Eddy, S.R. Stoyanov, E.E. Ebenso, *Int. J. Electrochem. Sci.* **5**, 1127 (2010)
47. Ayman M. Atta, Olfat E. El-Azabawy, H.S. Ismail, M.A. Hegazy, *Corros. Sci.* **53**, 1680 (2011)